

20-T, 120-cm-I.R. Target Magnet with Layer-Wound Resistive Magnet

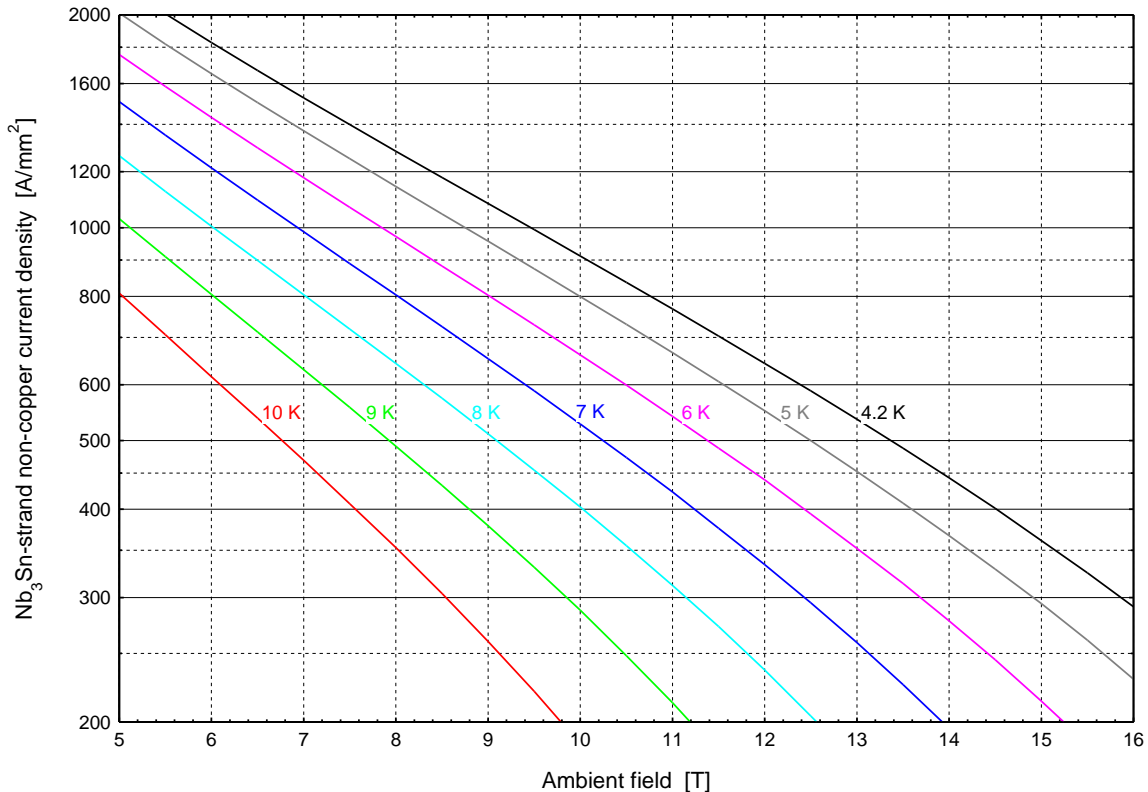
Bob Weggel 5/4-10/2011

This report presents designs for 20-tesla target magnets optimized by a computer program with major upgrades to its predictions of superconductor current density, magnet stresses and strains, and cost-optimization parameters. The field-and-temperature dependence of the non-copper current density in the Nb₃Sn in the strands of the superconducting cable is as shown in Fig. 1, generated by Eq. (1):

$$j(B, T) \cong \frac{46,630}{B} (1 - t^{1.247})^2 b^{0.437} (1 - b)^{1.727} \text{ [A/mm}^2\text{]}. \quad (1)$$

The magnetic flux density B is in teslas; t and b are, respectively, the normalized temperature T/T_c and normalized magnetic flux density $B/B_c(T)$. Equation (1) resembles that of "A general scaling relation for the critical current density in Nb₃Sn", by A Godecke, B ten Haken, H H J ten Kate and D C Larbalestier (2006 Supercond. Sci. Technol. **19** R100 doi: 10.1088/0953-2048/19/10/R02), but gives a much closer fit to the $j(B, T)$ data for Nb₃Sn of the ITER barrel magnet tabulated on page 645 of *Case Studies in Superconducting Magnets*, by Y. Iwasa. Fig. 2 plots the parameter $B_c(T) = 20.8 - 1.27 T - 0.0234 T^2$ needed by Eq. (1). Data points from which to generate the curve fit of Fig. 2 came from $T_c = 18.2 \text{ K}$ and the $j(B|T)$ curves of Fig. 3a&b, for which, by extrapolation, $j(B|T) = 0$ at [28.8 T, 1.8 K], [24.5 T, 4.2 K], and [16.1 T, 10 K].

Field and Temperature Dependence of Current Density of Nb₃Sn Strands



Bob Weggel 5/9/2011

Fig. 1: Non-copper current density vs. field and temperature for Nb₃Sn strands of ITER barrel magnet.

Temperature Dependence of Critical Field, B_c , of Nb_3Sn

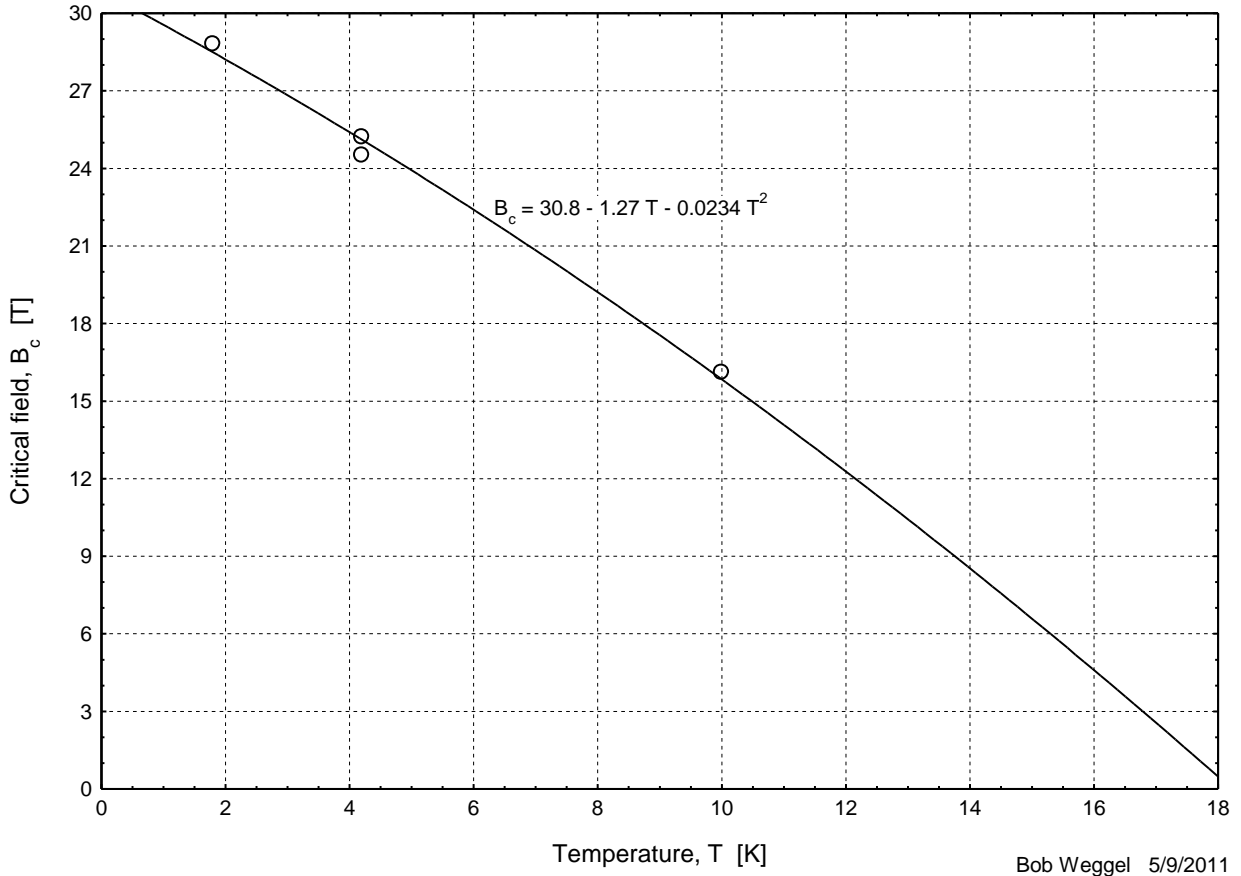


Fig. 2: Curve fit of data generated by Fig. 3a&b. $B_c(T) = 20.8 - 1.27 T - 0.0234 T^2$ teslas.

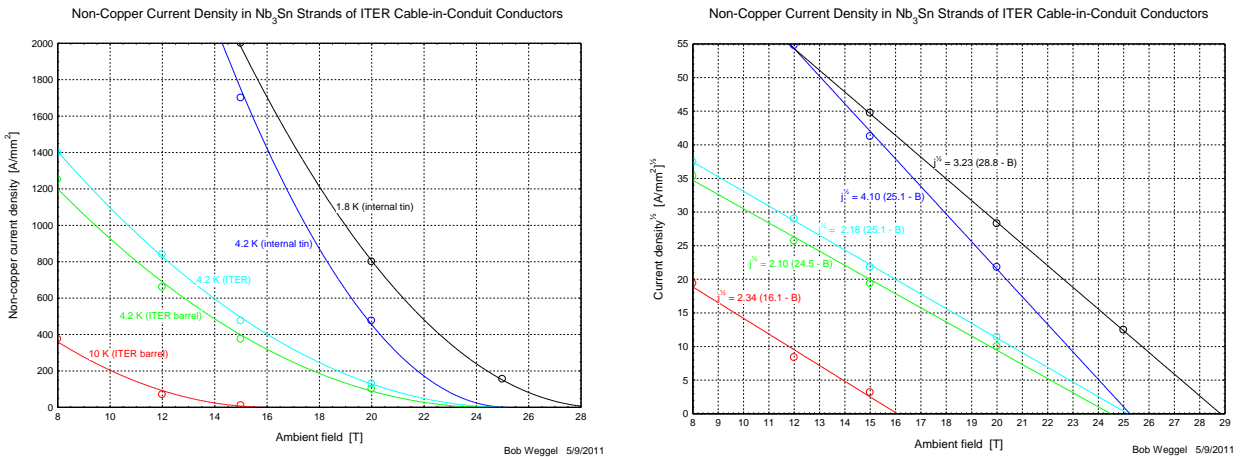
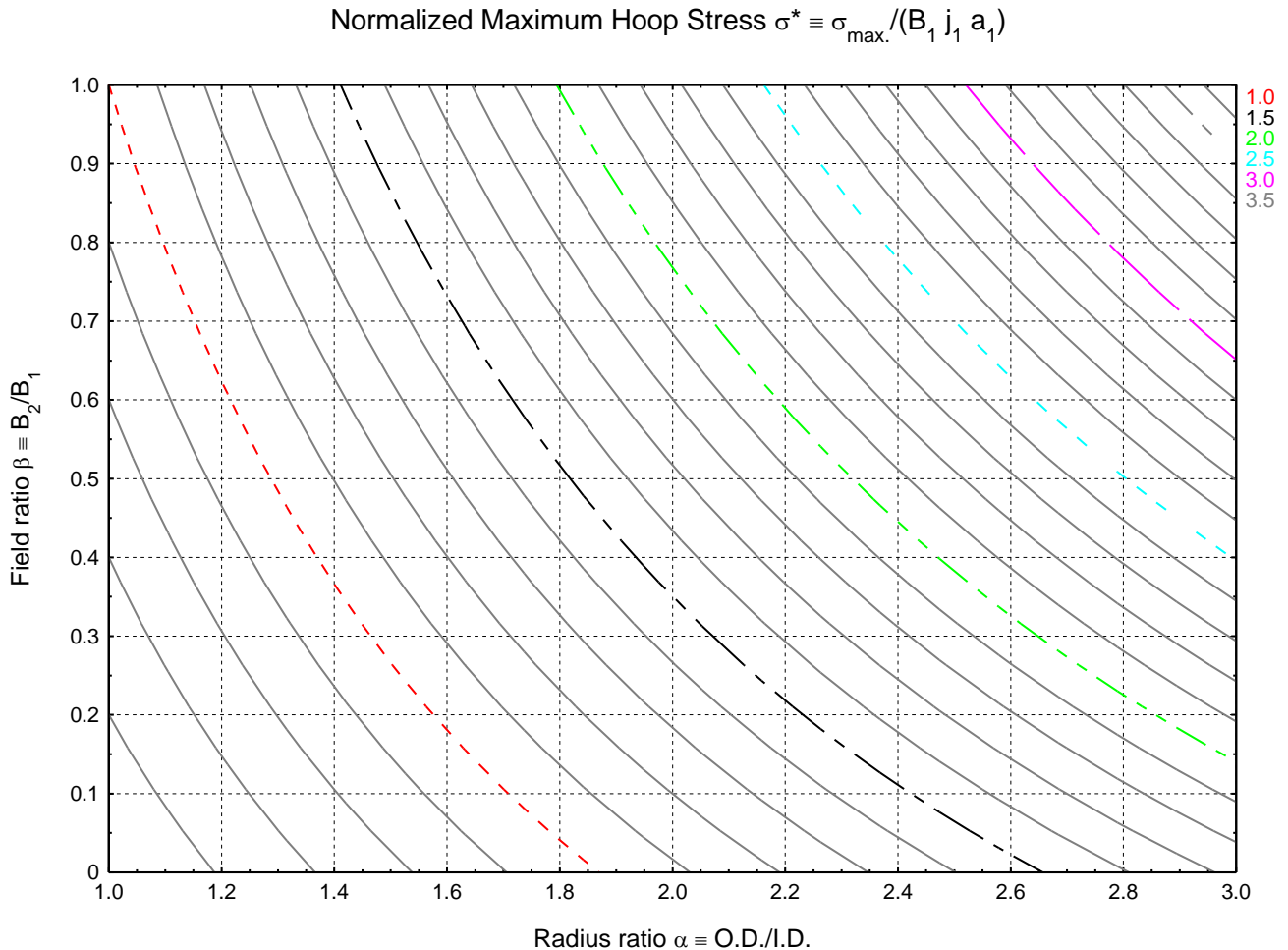


Fig. 3a&b: Curve fits of $j(B|T)$ by $j(B) \sim (B_c - B)^2$. Left: $j(B|T)$. Right: $\sqrt{j(B|T)}$. For ITER barrel conductor, extrapolation of the red curve to $j = 0$ gives $B_c = 16.1$ T at 10 K; extrapolation of the green curve gives $B_c = 24.5$ T at 4.2 K. For internal-tin conductor, $B_c = 25.1$ T at 4.2 K (blue curve) and 28.8 T at 1.8 K (black curve).

To predict the maximum stress (at the inner radius) in each solenoid, the computer program uses Eq. (5.35b) on p. 124 of *Solenoid Magnet Design* by Montgomery & Weggel or, equivalently, Eq. (3.77b) on p. 101 of *Case Studies in Superconducting Magnets*. The solenoid is of inner radius a_1 , outer radius a_2 , current density j , bore field B_1 , and external field B_2 , and is of isotropic material of Poisson's ratio $\nu = 0.3$. The predicted stress is:

$$\sigma_{max} = j \frac{(7a_1^2 + 14a_1a_2 + 85a_2^2)(B_1 + B_2) + 14(a_1^2B_1 + a_2^2B_2)}{120(a_1 + a_2)}$$

Fig. 4 presents the results. Note that for a radially-thin solenoid (radius ratio $\alpha \equiv a_2/a_1 \approx 1$), the peak stress is $\sigma_{max} = j_1 a_1 \langle B \rangle$, where $\langle B \rangle = (B_1+B_2)/2$, the average field in the windings. For solenoids of larger aspect ratio, $\sigma_{max} > j_1 a_1 (B_1+B_2)/2$ and is greater, even, than $j_1 [(a_1+a_2)/2] [(B_1+B_2)/2]$. For example, in a solenoid of radius ratio $\alpha = 1.6$ and field ratio $\beta = 0$ (appropriate for the most-upstream superconducting coil of a 20-T target magnet) the normalized stress $\sigma^* \equiv \sigma_{max} / (j_1 a_1 B_1)$ is 0.85, 31% greater than the 0.65 calculated from the mean field $0.5 B_1$ and the mean radius $(a_1+a_2)/2 = 1.3 a_1$. For a solenoid of radius ratio $\alpha = 2.8$ and field ratio $\beta = 0.7$ (appropriate for a pancake-wound resistive magnet of O.R. = 50 cm and I.R. = 17.5 cm) the normalized stress σ^* is 2.85, 76% higher than the $[(1+0.7)/2] \times [(1+2.8)/2] = 1.62$ predicted from the product of the mean radius and the mean magnetic field.



Bob Weggel 5/8/2011

Fig. 4: Normalized maximum hoop stress $\sigma^* \equiv \sigma_{max.} / (B_1 j_1 a_1)$ vs. radius ratio $\alpha \equiv \text{O.R./I.R.}$ & field ratio $\beta \equiv B_2/B_1$.

Fig. 5a-d, generated by a finite-element-method program, confirms that the magnet-optimization program does indeed generate designs in which the peak strain in every coil is very nearly the $\sim 0.4\%$ that should be acceptable for all the magnet materials: copper and stainless steel for the resistive coils, and Nb_3Sn , copper stabilizer and Incoloy 908 or other conduit material for the superconducting coils.

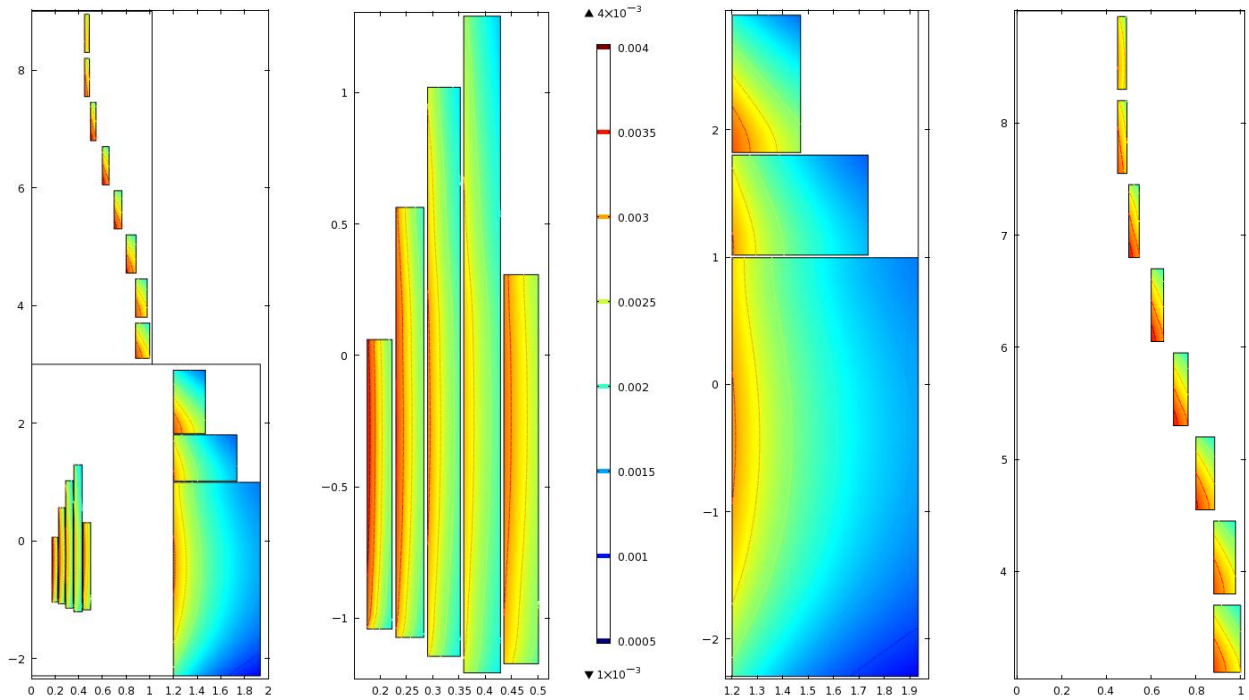


Fig. 5a-d: Hoop strain ϵ_{hoop} (color & contour lines) of 20-T target magnet with layer-wound resistive coils and upstream superconducting (SC) coils of 120-cm inner radius. Total stored energy = 2.88 GJ. Resistive magnet has five nested two-layer coils of MgO-insulated hollow conductor, graded from 23.8 mm square Japanese-Hadron-Facility hollow conductor (innermost coil) to ~ 35 mm square (outer two coils); supporting each coil is a stainless-steel tube or wrap of 600 MPa design stress. Field contribution = 5.3 T at 12.0 MW; field homogeneity = 3.3% peak-to-peak; $\Delta T_{\text{max}} = 70$ °C with water flow of 59 liters/sec ($\Delta P = 40$ atm, 4 hydraulic paths per layer). The most-upstream SC coil has an outer radius of 193 cm, a length of 3.3 meters, a weight of 130 metric tons, and is 9% Nb_3Sn , 51% steel, and 32% copper+helium and 8% insulation. The endmost coil shown is 1.4% superconductor, 4.5% steel, 75% copper+helium, and 19% insulation. a) Entire magnet upstream of 9 m. b) Resistive magnet. c) Upstream SC coils. d) Downstream SC coils.

Fig. 6 shows that the magnet of Fig. 5 generates an on-axis field profile that matches very closely the desired profile. Fig. 7 plots parameters of magnets optimized for minimum yearly cost of operation for a duty cycle ranging from 32% to 63% ($1\text{-}3 \times 10^7$ sec/yr). The cost optimization uses parameters based on values from the NHMFL web site: 1) Power = \$121/MW-hr; 2) Fabricated copper and steel is \$400/kg (nearly twice the average for non-superconducting NHMFL magnets, to account for inflation and that the optimization ignores the mass of components such as shielding and cryostats; 3) The cost of superconducting magnets is 2 to 2½ times that of non-superconducting magnets; and 4) Amortization of capital investments is at 10% per year.

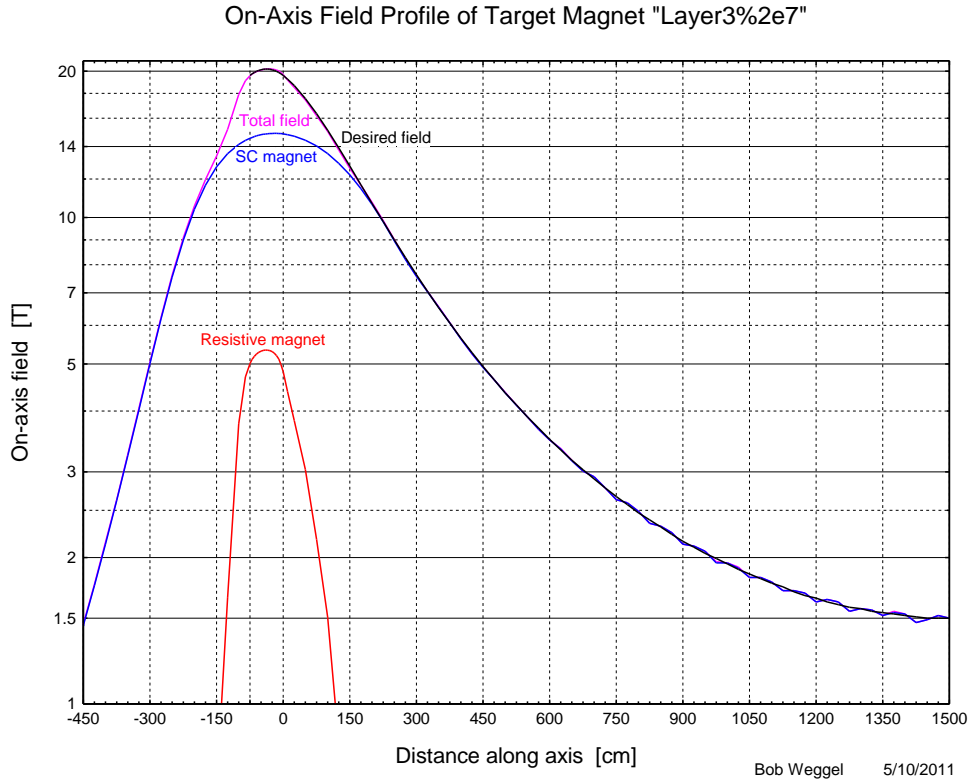


Fig. 6: On-axis field profiles of superconducting magnet and layer-wound resistive magnet of 20-T target magnet optimized for 2×10^7 sec/yr of operation.

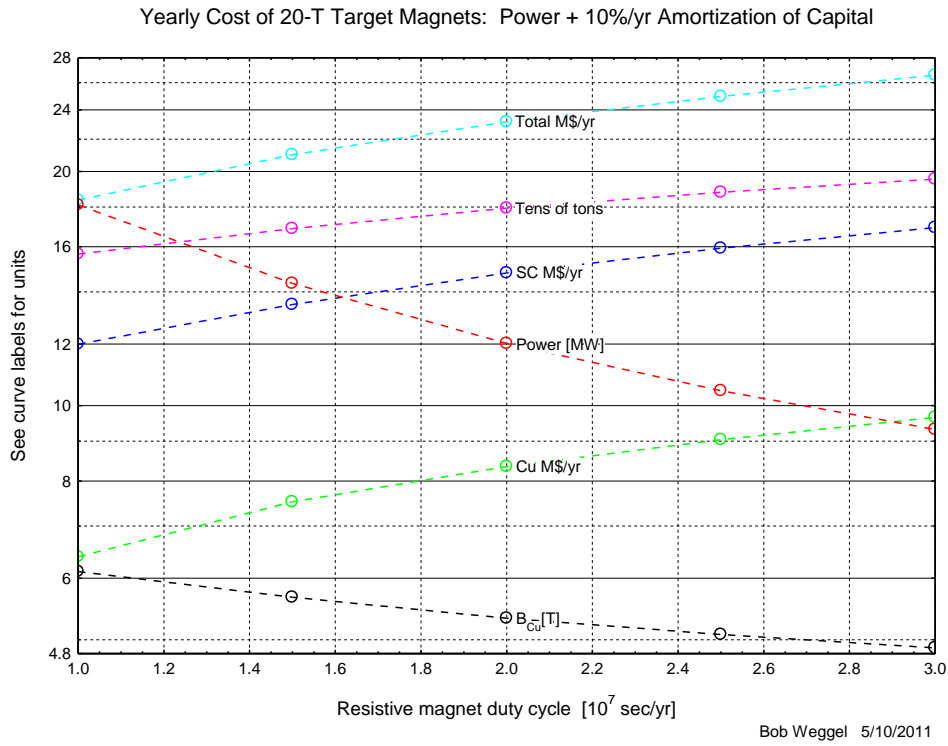


Fig. 7: Power, field allocation, mass, & yearly cost of optimized 20-T target magnets: duty cycle = $1-3 \times 10^7$ sec/yr.

On-Axis Field of 15.30-kA, 18.1-MW Target Magnet "Layer3%1e7" at 11.44 kA, 9.3 MW

